CESR Performance and Upgrade Status*

Stuart Henderson † for the CESR Operations Group
Laboratory of Nuclear Studies, Cornell University, Ithaca NY, 14853, USA

Abstract

The performance of the Cornell Electron Storage Ring (CESR) e^+e^- collider will be reviewed. CESR collides trains of closely spaced bunches at a small horizontal crossing angle. At present, CESR collides 36 bunches per beam at total currents up to 550 mA. A peak luminosity of 8.3×10^{32} cm^{-2} sec^{-1} has been achieved. A longitudinal beam instability due to higher-order-modes in CESR's normal conducting RF cavities has limited total beam currents. This current limitation has been addressed with wideband multibunch feedback and replacement of CESR's normal-conducting cavities with low-impedance single-cell superconducting cavities. The status of the longitudinal beam stability is described and experience with SRF in operation is discussed. Finally, plans are presented for a new interaction region optics (CESR Phase III) based on high-gradient superconducting quadrupoles which will allow a reduction in $\beta_v^\star$ from the present 19 mm to as low as 7 mm. The superconducting RF system will support a beam current of 1A at a bunch length of 13mm, giving a peak luminosity of 2×10^{33} cm^{-2} sec^{-1}.

1 INTRODUCTION

The Cornell Electron Storage Ring (CESR) is a single-ring symmetric e^+e^- collider operating on and near the $\Upsilon(4S)$ resonance ($E \simeq 5.3$ GeV). At present, each beam consists of 36 bunches arranged in 9 bunch trains, each of which is populated with 4 bunches spaced by 14 ns. The beams collide with a small horizontal crossing angle (± 2 mrad) at a single interaction point where the CLEO detector is located. CESR has achieved a peak luminosity of 8.3×10^{32} cm^{-2} sec^{-1}, a peak total beam current of 550 mA and a beam-beam tunshift parameter of $\xi_v = 0.05$.

For the last four years CESR's beam current has been limited by two factors: a longitudinal coupled bunch instability due to high-Q parasitic modes in the normal conducting RF cavities and limitations related to the high-current operation of the RF system. The development of a longitudinal feedback system [1] has allowed CESR to operate at total beam currents which are a factor of two above the instability threshold currents. In order to provide higher current capability as well as to mitigate the longitudinal instability, we began in 1997 to replace CESR's 5-cell normal conducting (NRF) cavities with single cell low-impedance superconducting cavities (SRF) [2, 3]. With the last of CESR's normal conducting cavities removed, we observed increases in longitudinal instability thresholds of as much as 50% in some bunch spacings.

In order to reach a total beam current of 1A and provide a smaller $\beta_v^\star$, new interaction region (IR) optics will be installed in 2000. The new interaction region magnets consist of permanent magnet quadrupoles and high-gradient superconducting magnets [4]. The high-gradient capability of the superconducting RF system will allow a reduction in bunch length from the present 19mm to 13mm and the new IR quadrupoles will allow a corresponding decrease in $\beta_v^\star$. In this third phase of CESR operation (CESR Phase III) we expect to reach peak luminosities of 2×10^{33} cm^{-2} sec^{-1}.

2 CESR PHASE II

Since CESR is a single-ring collider, the counter-rotating beams must be separated except at a single interaction point. The beams follow "pretzel" orbits established with a set of four horizontal separators, as shown in Figure 1. By designing a pretzel having maxima at the parasitic crossing locations, bunch trains are separated in the machine arcs. Separation of bunches in opposing beams in the IR is achieved by colliding the beams at a small horizontal angle; the crossing angle is chosen to provide adequate separation at the nearest parasitic crossing point.

The tune shift arising from the long-range beam-beam force at a parasitic crossing is

$$\Delta Q_{x,y} \propto \frac{I\beta_{x,y}}{(d+x)^2} \quad (1)$$

where I is the bunch current, d is the separation between nominal closed orbits and x is the displacement of a particle from the nominal orbit. Minimizing the impact of parasitic crossings requires reduced β's, large separations and small ratios of beamsize to separation.

The minimum bunch spacing within a train of bunches is limited by the nearest parasitic crossing point in the IR, where the separation is small and the β is typically large. On the other hand, the length of a bunch train is determined by those parasitic crossings in the arcs with the least separation. As the train length occupies a greater fraction of a horizontal betatron wavelength, the separation for the trailing bunch becomes smaller since the pretzel amplitude eventually limits due to aperture constraints. At present, CESR's train length is limited to 56 ns ($\sim$ 40% of a betatron half-wavelength).

* Work supported by the National Science Foundation.
† Email: sdh9@cornell.edu

The present CESR optics (shown in Figure 2) were designed for 9 trains of 3 bunches per train spaced by 28 ns with 11 mA/bunch. A smaller bunch spacing *at design bunch currents* is precluded by the large β's near the IP. We found, however, that with smaller bunch currents we were able to operate with 4 or 5 bunches per train, spaced by 14 ns. CESR has operated since November 1998 with 4 bunches per train separated by 14 ns with 6-7 mA/bunch.

Parameters related to CESR's present configuration, which we refer to as CESR Phase II, are shown in Table 1. Underway are two modifications to the optics which will allow more current to be stored. First, we found that with the addition of a pair of quadrupoles an optics can be designed which allows 6 bunches per train (70 ns train length) instead of the present 5. Second, a new interaction region optics based on superconducting quadrupoles will be installed in 2000. The new IR optics, shown in Figure 2, have been optimized for 14 ns spaced bunch trains, and has β's at the IR parasitic crossing points (spaced at 2.1 m intervals) which are comparable to those in the arcs. This new configuration, which we refer to as CESR Phase III, will be discussed in detail below. In addition, recent machine studies experiments show that it may be possible to further reduce the spacing between bunches in a train to as little as 6 ns, albeit with smaller per bunch currents. The flexibility to increase the number of bunches and reduce the bunch current may be important for reaching the Phase III beam current goal. In this case, as many as 10 bunches per train may be possible.

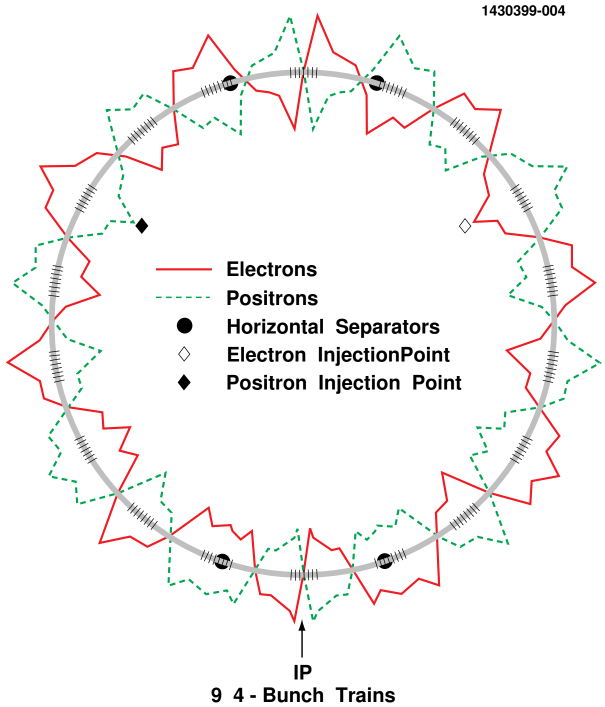

Figure 1: Pretzel Orbit in CESR. The tic marks denote parasitic crossing points for 9 trains and 4 bunches per train spaced by 14ns. The peak pretzel amplitude is ~2 cm.

	Phase II Jan 1999	Phase III May 2000
Energy (GeV)	5.289	5.289
Circumference (m)	768.4	768.4
Beam Current (A)	0.55	1.0
Bunch trains	9	9
Bunches/train	4	6-10
Bunch spacing (ns)	14	6-14
5-cell copper cavities	2	0
Single cell SRF cavities	2	4
RF Voltage (MV)	6.0	7-12
RF Power (MW)	0.7	1.3
Q_x	10.53	10.53
Q_y	9.60	9.60
θ_c (mrad)	2.2	2.7
β_v (mm)	18	13
σ_z (mm)	19	13
ξ_v	0.05	0.05
$\mathcal{L}$ (10^{33} cm^{-2} sec^{-1})	0.83	2.0

Table 1: CESR Parameters for Phase II and Phase III. The Phase II parameters are actual operating values as of January 1999.

3 CESR PERFORMANCE

The history of CESR's peak luminosity is shown in Figure 3. CESR has reached a peak luminosity of 8.3×10^{32} cm^{-2} sec^{-1}. CESR's monthly integrated luminosity is shown in

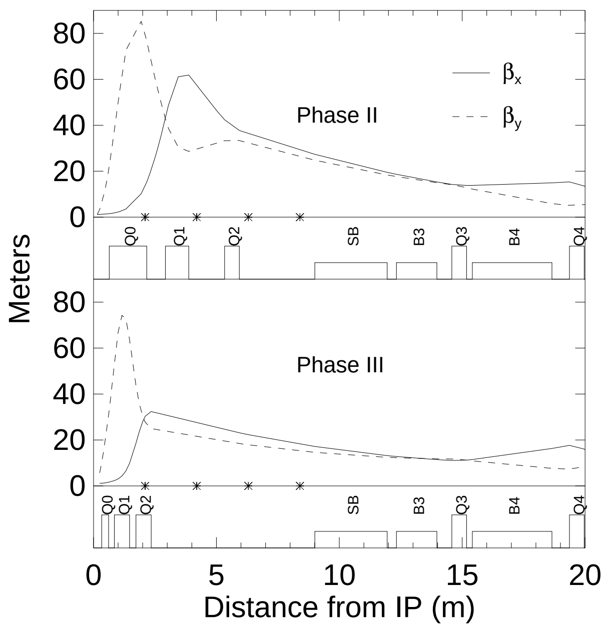

Figure 2: CESR Phase II and Phase III interaction region optics. Parasitic crossing points for 14 ns spaced bunch trains are denoted by stars.

Figure 4. In CESR's best month, 0.75 fb^{-1} was delivered. CESR's highest daily integrated luminosity is 40.2 pb^{-1}. CESR delivered 3.4 fb^{-1} in 1997 and 4.4 fb^{-1} in 1998.

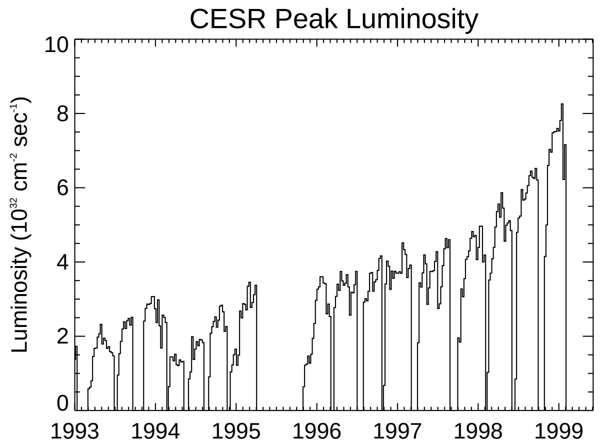

Figure 3: CESR peak luminosity history.

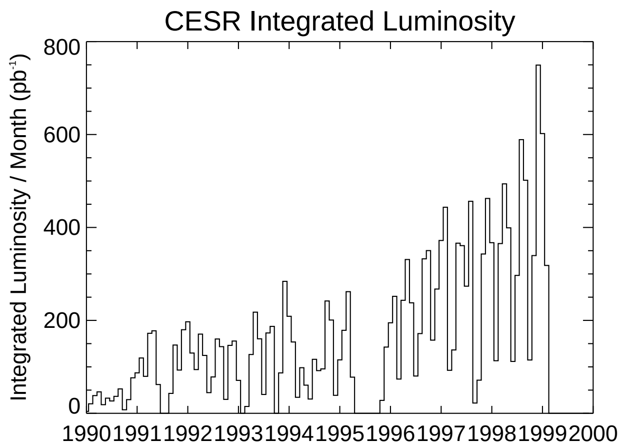

Figure 4: CESR monthly integrated luminosity history.

Clearly, integrated luminosity is the single most important measure of performance of a "factory" collider. A factory mode of operation requires maintaining a large instantaneous peak luminosity and operation near peak performance over long periods of time. One way of quantifying the operational efficiency for a given period of time, ρ_T, is through the ratio of average to peak luminosity:

$$\rho_T = \frac{\int_T \mathcal{L}\, dt}{\hat{\mathcal{L}} \times T} \qquad (2)$$

ρ_T is less than 100% due to luminosity lifetime, machine downtime, injection and less than peak luminosity performance. CESR's operating efficiency in recent years is as follows: 24% (1996), 27% (1997) and 24% (1998). A large portion of the time is spent in machine studies ($\sim$25% of running time) or in scheduled maintenance and upgrades (20-25%).

At the end of a high-energy-physics run, the electron beam is removed, the positron current is topped off and electrons are injected. During the last HEP run period, this process took $\sim$10 minutes on average for $\sim$500 mA total colliding beam current. The average luminosity lifetime over the last two months of HEP running was 113 minutes. In order to see directly the effect of luminosity lifetime and time spent injecting, we may form the efficiency ratio excluding machine studies and maintenance periods. Calculated in this way yields an operating efficiency of 51% in 1997 and 50% in 1998.

4 BEAM CURRENT LIMITATIONS

CESR's beam current history is shown in Figure 5. Over the last several years CESR's beam current has been limited primarily by a longitudinal multibunch instability and by RF system trips related to high-current operation.

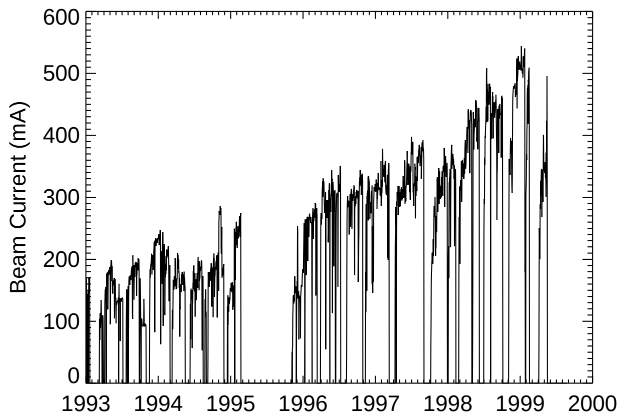

Figure 5: CESR peak beam current history.

4.1 Longitudinal Beam Stability

In early 1996 CESR beam currents began to be limited by a longitudinal coupled bunch instability due to high-Q parasitic modes in CESR's normal conducting RF cavities [6, 7]. In addition, a coupled bunch mode was excited by the beam-cavity fundamental interaction at large beam currents due to the large frequency detuning of the normal-conducting cavities needed to compensate beam loading [10].

It was found that the longitudinal instability has a beam current threshold behaviour which depends in detail on the bunch pattern. Observation of the frequency spectrum of a beam position monitor showed the rapid growth of synchrotron sidebands of revolution harmonics once the threshold current is reached. Continued filling of beam current eventually lead to beamloss, although operation $\sim$10% above threshold was possible.

Figure 6 shows a set of longitudinal instability threshold measurements for a positron beam and for two beams with 2,3,4 and 5 bunches in 9 trains with varying bunch patterns.

(This data was taken with 2 NRF cavities and 2 SRF cavi-

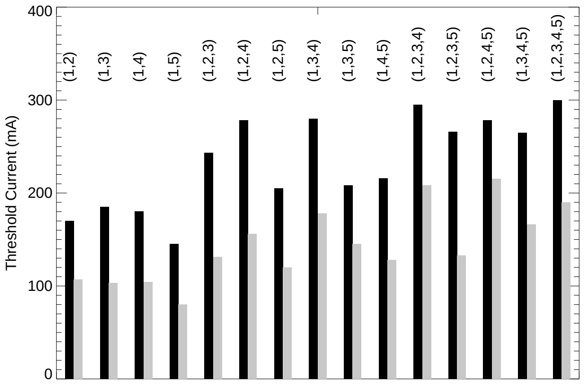

Figure 6: Longitudinal instability threshold currents versus bunch pattern for single beams (light) and two beams (dark). The cases are labelled by the 14 ns bucket in each train which is occupied. For example, (1,2,3,5) denotes 9 trains of 4 bunches each, where the first three bunches are separated by 14 ns, and last is separated by 28 ns. This data was taken when CESR operated with 2 NRF and 2 SRF cavities.

ties; see below). The cases are labelled by the 14ns bucket in each train which is occupied. The single and two beam current thresholds differ by up to a factor of two suggesting some cancellation in the RF fields responsible for the instability when two beams are present. There is also a factor of $\sim$2 variation within the two beam thresholds. As a result, we have generally chosen a bunch pattern with the highest instability threshold for CESR operation, and have operated in recent years with $9 \times 2, 9 \times 3$ and 9×4 configurations.

Several observations were made which are consistent with the normal-conducting cavities as having the impedance responsible for the instability. First, it was found that the instability thresholds were sensitive to horizontal orbit through the cavities. Secondly, small changes in cavity temperature (of the order of a few $^\circ C$) could change the thresholds at the $\sim$5% level. Finally, high-Q modes were seen in the frequency spectra of beam-induced signals on the cavity field probes. Modes were observed in the frequency range 1.8-3 GHz with $Q > 10000$. These modes therefore have decay times of 1-1.8 μs, long enough to couple motion between trains of bunches (the bunch trains are separated by 280 ns).

The limitations from longitudinal beam stability have been addressed in two ways. First, a digital multibunch longitudinal feedback system has been developed. This system consists of a phase receiver, digital filtering and signal processing and a power amplifier which drives a stripline kicker [1]. The output of the longitudinal feedback processor is combined with the output of the horizontal feedback system to drive a horizontal stripline kicker differentially. The horizontal kicker provides longitudinal damping via dispersion at the kicker location. In addition, a low-Q 1.1 GHz longitudinal feedback cavity kicker has been built, based on a design used at DAΦNE. The cavity was installed and tested with beam during the last running period. Narrowband feedback acting on the RF drive was used to damp the coupled-bunch mode excited at the highest beam currents by the large frequency detuning of the normal conducting cavities. With the longitudinal feedback in operation, we have been able to operate at beam currents a factor of 2.3 above the instability threshold current.

4.2 *Superconducting RF*

The second prong in the attack on longitudinal beam instability has been to replace CESR's normal conducting 5-cell RF cavities with low-impedance single-cell superconducting cavities [5, 2, 3]. A single superconducting cavity has $\sim$6% of the impedance at the cavity fundamental of the 5-cell normal conducting cavity that it replaces. Furthermore, the cell geometry and large inner radius reduce the R/Q of the HOM's to $\sim$1/10 that of a normal-conducting CESR cell. The longitudinal HOM's propagate out of the cavity in the round beam pipe, as do all but the two lowest frequency transverse modes. A fluted beam tube on the other end of the cavity guides these transverse modes outside the cryostat. All HOM power propagates outside the cryogenic environment where room temperature ferrite loads are placed to extract the HOM power. The Q's of all HOM's are less than 100. RF power is delivered to the cavity through a ceramic waveguide window to a waveguide input coupler.

The RF system replacement began in 1997 and the final SRF cavity was installed in September 1999 and awaits commissioning. Since we have performed a staged replacement of the normal conducting RF, we have been able to study the impact on longitudinal instability thresholds at each step. Figures 7 and 8 show a comparison of instability threshold measurements in 9×4 and 9×5 bunch patterns for 4 NRF, 2 NRF/2 SRF and 3 SRF cavities for single and two beams. As is seen, removal of the final two NRF cavities and replacement with a single SRF has yielded the greatest gain in instability thresholds. For some single-beam 9×4 bunch patterns, thresholds have increased by $\sim 80\%$, and some two beam thresholds have increased by $\sim 50\%$. We observed during the 3 SRF cavity running period that the amplitude of synchrotron sidebands above threshold are self-limiting; it is possible to store current well above threshold with no increase in oscillation amplitude. In fact, we were able to store 500 mA total current in two beams without the use of longitudinal feedback. Furthermore, the existing longitudinal feedback system provided more than enough damping to stabilize the small longitudinal motion.

The instability threshold increases with the NRF cavities removed are not quite as dramatic as we might have expected. A detailed calculation and comparison to thresh-

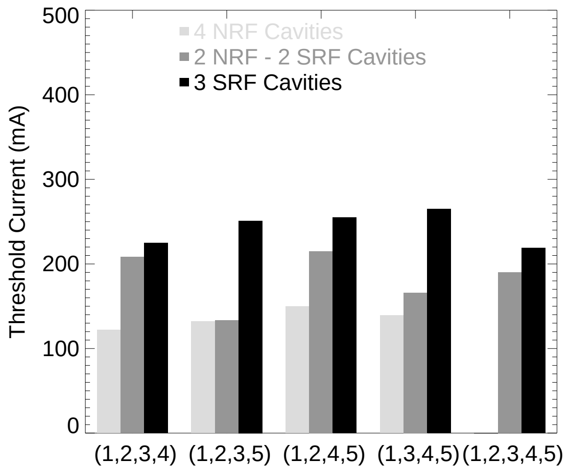

Figure 7: Single beam longitudinal instability threshold measurements in 9×4 and 9×5 bunch patterns for different configurations of the RF system.

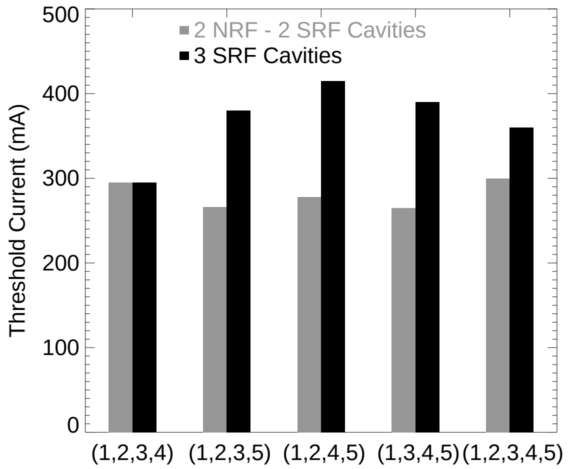

Figure 8: Two beam longitudinal instability threshold measurements in 9×4 and 9×5 bunch patterns for different configurations of the RF system.

old data has been performed [7]. The higher-order-mode frequency spectra from the field probes of all the accessible NRF cells were recorded and analyzed to fit observed peaks and identify modes. These measured higher-order-modes were used as input to the program MBI[8] to compute the growth rate of the most unstable eigenmode. The analysis showed good agreement for the case of 4 NRF cavities and 3 NRF/1 SRF, but began to worsen for the 2 NRF/2 SRF case. These results suggest that as NRF cavities are removed, the impedance of the rest of the ring becomes more important and then dominates the longitudinal dynamics when all NRF cavities are removed. Recent measurements and calculations suggest that HOM's in the electrostatic separators may produce longitudinal instability thresholds in the range of present observations [9].

We estimate that the present feedback system has adequate damping to provide longitudinal stability to beam currents in the range 760 - 970 mA. With the use of the longitudinal feedback cavity the longitudinal kick delivered to the beam is increased by a factor of 3-5 providing beam stability for at least $I > 2.3$A.

Finally, it should be mentioned that the coupled bunch mode excited by the large frequency detuning at high beam currents in the NRF system is not an issue with an SRF system due to the narrow impedance of the fundamental mode and the reduced detuning with beam current.

4.3 RF System Operation

The first SRF cavity (E2) was installed in September 1997. During the commissioning phase, CESR beam currents were limited by travelling wave power (forward power - reflected power) which could be tolerated by the cavity. We observed high vacuum trips at rather repeatable power levels due to gas evolution brought on by multipacting in the window and coupler region. The power delivered to the beam by each of the three superconducting cavities is shown in Figure 9. Two processing techniques have proven useful in raising the travelling wave power limits. We found that by processing the cavity on resonance without beam using pulsed power that the travelling wave power limit with beam could be raised from 100 kW to 140 kW. Another processing technique that has been useful is to process with stored beam and continue to raise the beam power by adjusting the relative phase between the two RF stations. A software program has been developed to automatically adjust the relative phase while monitoring RF vacuum signals.

A second variety of vacuum trip arose from RF heating of the waveguide thermal transition section. Such vacuum events showed a measurable temperature rise on the transition section, and were accompanied by a large release of hydrogen as observed on an RGA. Presumably cryosorbed hydrogren was released as the surface was heated. We found after warming up the cavity to room temperature and baking the RF window that the subsequent transmitted power limit was raised to 180 kW. After another warmup the E2 power delivered to the beam eventually reached 212 kW.

Experience with the first SRF cavity suggested modifications to the cryomodule design and handling procedures which were incorporated into subsequent cavities. The second cavity (E1) was installed in October of 1998 and reached 220 kW power delivered to the beam within one month of operation. The third cavity, installed in March 1999 reached 260 kW within 6 weeks of operation. The last SRF cavity was installed in September 1999 and awaits commissioning in November 1999.

Typically, the SRF cavities have operated in the range of 5-7 MV/m. In tests prior to installation, four cavities

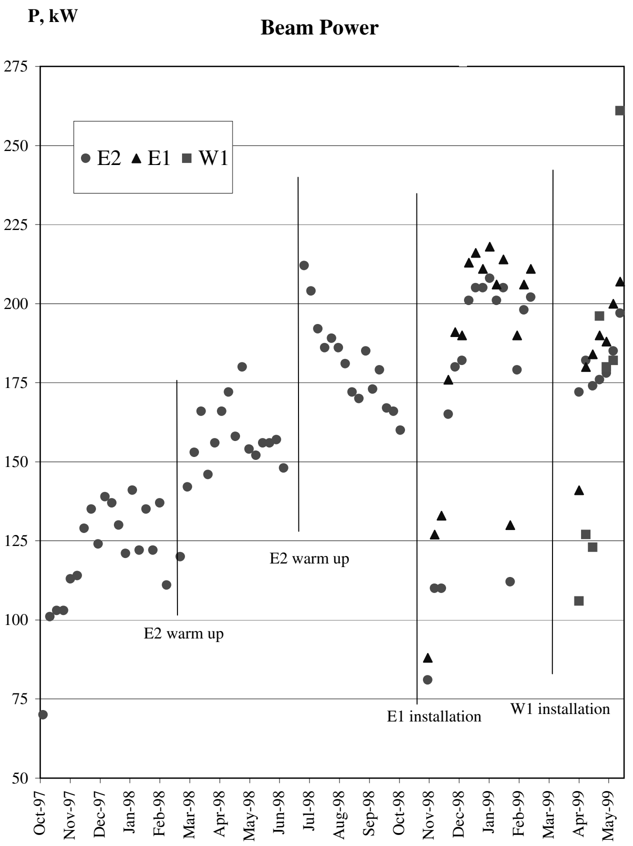

Figure 9: RF power delivered to the beam by the three SRF cavities.

reached accelerating gradients of 12 MV/m, 11 MV/m, 10 MV/m and 7.8 MV/m. This high-gradient capability of the SRF system will allow a reduction in bunch length from 19 mm to 13 mm. The SRF system is capable of supporting 1A total current by delivering 325 kW per cavity. A new 800 kW klystron has been installed to drive two cavities and two 375 kW klystrons will drive the other two.

5 BEAM-BEAM PERFORMANCE

The luminosity and beam-beam tuneshift parameter vs. bunch current are shown in Figure 10. The Figure shows a superposition of data acquired in a single day. The beam-beam tuneshift parameter saturates at ∼0.05 at ∼6 mA/bunch. A number of improvements over the last several years have resulted in improved beam-beam performance. Some of these are described here. For a more detailed discussion see [11] in these proceedings.

In the past, β-functions were measured by modulating quadrupole strengths. This method had difficulties associated with magnet hysterisis and saturation, and could be operationally difficult (due to beamloss). Recently a betatron phase and transverse coupling diagnostic system was implemented at CESR [12]. This system provides data which is far superior to the original. This system, together with an analysis package (see [13] in these proceedings) has pro-

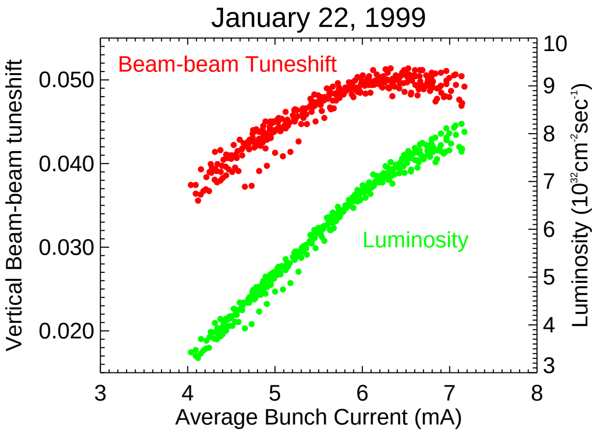

Figure 10: Vertical beam-beam tuneshift parameter, ξ_v, and luminosity versus bunch current.

vided the capability of routine lattice loading and correction, yielding RMS betatron phase errors less than 2°. This analysis system has also aided in diagnosing and correcting errors associated with the solenoid coupling compensation. We have found that as our ability to correct the linear lattice and transverse coupling improves, so does the beam-beam tuneshift parameter.

Since the beams are generally far from the centerline and displaced in opposite directions due to the electrostatic pretzel, magnetic alignment, magnetic field errors and non-linear fields must be carefully considered. Non-linear fringe fields which might otherwise be acceptable for on-axis beams may influence the beams in pretzel operation. We recently completed modifications to all the sextupole pole-tips to improve their field quality [14].

Similarly, large corrector strengths needed to compensate for quadrupole misalignment may introduce non-linear fields at locations with large pretzel amplitude. More troublesome are field errors which produce differential effects for electrons and positrons. As part of our general maintenance program, the quadrupole heights, radial positions and rotations are routinely measured and aligned during maintenance periods. An average increase in the beam-beam tuneshift parameter of 11 ± 6% was realized during maintenance periods in which CESR elements were aligned compared to a loss of 4 ± 5% when no alignment was performed [15].

Since the beams are differentially displaced in the sextupole magnets, the effect on the lattice functions is different for the two beams. We have found the beam-beam parameter to be quite sensitive to the details of the sextupole distribition. An algorithm has been developed based on dynamic aperture modelling in which the amplitude and energy dependence of β functions are minimized and the vertical amplitude dependence of coupling parameters are minimized [16].

Finally, the implementation of a fast vertical beam-beam luminosity monitor [17] has proven to be invaluable to the luminosity tune-up operation. The monitor is used together with real-time tuning optimization software to maintain the luminosity during a run in an attempt to compensate for effects associated with decreasing bunch currents.

6 CESR PHASE III

With the installation of new interaction region optics [4] in 2000, CESR will enter Phase III of its operation. After the installation of the last superconducting RF cavity, the limitation to CESR's total beam current will probably be the destructive effects of the nearest parasitic crossing point in the IR (located at 2.1 m) as bunch currents are increased in 9×4 or 9×5 operation. The Phase III IR has been optimized specifically for 14 ns bunch trains. The design philosophy is to move all the IR focussing elements as close to the IP as possible, so that the β's at the nearest crossing point are reduced. A combination of short focal length and large aperture are optimum in this respect, and best implemented with insertion optics consisting of two pairs of high-gradient superconducting (SC) quadrupoles and two pairs of permanent magnet quadrupoles. The interaction region optics and layout are shown in Figure 2. The β's at the nearest crossing point are $\beta_x \simeq \beta_y \simeq 30$ m which is comparable to those found at parasitic crossings in the arcs.

The insertion optics consist of seven magnets on each side of the IP. At 34 cm from the IP is a short NdFeB permanent magnet quadrupole. A single cryostat contains the remaining magnets: a quadrupole doublet (Q1 and Q2), a pair of skew quadrupoles concentrically wound on top of each main quadrupole coil, and two dipole correctors concentrically wound on top of the skew quadrupole to provide vertical deflection. The main quadrupole coils can achieve gradients of 48 T/m at 1225 A. The skew quadrupole field is 10% that of the main quadrupole, and is needed to rotate the quadrupole field for the detector solenoid compensation. The vertical dipole correctors will provide alignment of the magnetic centers within the physical aperture. The cryostat has a warm bore ID of 145 mm. The SC quad cryostat is supported and aligned by eccentrically driven cam bearings held by support rails which are mounted to the CLEO detector steel. We expect to receive two complete SC quad packages in their cryostats by the end of 1999.

In addition to new IR magnets, new vacuum system components are required. A new beryllium central beampipe, detector background shielding and vacuum pumping will be installed. Pressure in the IR will be maintained below 3.5 nTorr at 1A total current by massive titanium sublimation pumping.

The Phase III design parameters are shown in Table 1. Since the superconducting RF system will allow a reduction in bunch length from the present 19 mm to 13 mm, luminosity gain can be realized with a corresponding decrease in $\beta_v^\star$. Considerable flexibility in IR optics is afforded by the high-gradient SC quadrupoles. In fact, optics have been designed with $\beta_v^\star$ as small as 7 mm. In addition, round-beam optics with $\beta_v^\star = \beta_h^\star = 3$ cm are possible.

7 CONCLUSIONS

The status of CESR performance has been reviewed. CESR luminosity continues to grow as beam current limitations are addressed. Longitudinal feedback has allowed operation at beam currents a factor of $\sim$2 above longitudinal instability thresholds. All of CESR's normal conducting RF cavities have been replaced with single-cell low-impedance superconducting cavities, and longitudinal instability thresholds have improved as a result. The high-gradient capability of the SRF system, coupled with new interaction region optics will allow CESR to operate at a peak luminosity of 2×10^{33} cm^{-2} sec^{-1}.

8 ACKNOWLEDGMENTS

The hard work and dedication of the CESR staff is greatly appreciated. The author would like to thank David Rubin and Sergey Belomestnykh for useful discussions.

9 REFERENCES

[1] J. Sikora *et. al.* Proc. Part. Acc. Conf. 1999, New York, NY, p. 1115.

[2] S. Belomestnykh, Proc. Part. Acc. Conf. 1999, New York, NY, p.272

[3] S. Belomestnykh *et. al.*, Proc. Part. Acc. Conf. 1999, New York, NY, p.980

[4] S. Henderson *et. al.*, Proc. Part. Acc. Conf. 1999, New York, NY, p.3221.

[5] CESR-B Conceptual Design for a B-factory Based on CESR, Cornell, 1993.

[6] M. Billing, Proc. Part. Acc. Conf. 1997, Vancouver BC, p.2317

[7] M.G. Billing and S. Belomestnykh, Proc. Part. Acc. Conf. 1999, New York, NY, p. 1112

[8] M.M. Karliner *et. al.*, Proc. Third Advanced ICFA Workshop on Beam-Beam Effects in Circular Colliders, Novosibirsk, 1989, p.131.

[9] S. Temnykh, private communication.

[10] D. Fromowitz, Proc. Part. Acc. Conf. 1999, New York, NY

[11] D. Rice, in these proceedings.

[12] D. Sagan, D. Rubin and S. Greenwald, Proc. 1996 Euro. Part. Acc. Conf. p. 1335.

[13] S. Henderson and D. Sagan in these proceedings.

[14] A. Mikhailichenko, Cornell CBN 98-2.

[15] R. Holtzapple and D. Rice, Proc. Part. Acc. Conf. 1999, New York, NY, p.2972.

[16] S.B. Peck and D. Rubin, Proc. Part. Acc. Conf. 1999, New York, NY, p.285

[17] D. Sagan, J. Sikora and S. Henderson, Proc. Part. Acc. Conf. 1997, Vancouver, BC, p.1765.